Overcoming Myelosuppression Due to Synthetic Lethal Toxicity in FLT3-Targeted Acute Myeloid Leukemia Therapy

Alexander A. Warkentin[1], Michael S. Lopez[1], Elisabeth A. Lasater[2], Kimberly Lin[2], Bai-Liang He[3], Anskar Y. H. Leung[3], Catherine C. Smith[2*], Neil P. Shah[2*], Kevan M. Shokat[1*]

To whom correspondence should be addressed: kevan.shokat@ucsf.edu, nshah@medicine.ucsf.edu, csmith@medicine.ucsf.edu

[1]*Howard Hughes Medical Institute and Department of Cellular and Molecular Pharmacology, University of California, San Francisco, California, USA*

[2]*Division of Hematology/Oncology, University of California, San Francisco, California, USA*

[3]*Division of Haematology, Department of Medicine, Li Ka Shing Faculty of Medicine, The University of Hong Kong, Pokfulam, Hong Kong*

Competing financial interests. Authors declare no competing financial interests.

Abstract: Activating mutations in FLT3 confer poor prognosis for individuals with Acute Myeloid Leukemia (AML). Clinically active investigational FLT3 inhibitors can

achieve complete remissions, but their utility has been hampered by acquired resistance and myelosuppression attributed to a "synthetic lethal toxicity" arising from simultaneous inhibition of FLT3 and KIT. We report a novel chemical strategy for selective FLT3 inhibition while avoiding KIT inhibition with the staurosporine analog, Star 27. Star 27 maintains potency against FLT3 in proliferation assays of FLT3-transformed cells compared to KIT-dependent cells, shows no toxicity towards normal human hematopoiesis at concentrations that inhibit primary FLT3-mutant AML blast growth, and is active against mutations that confer resistance to clinical inhibitors. As a more complete understanding of kinase networks emerges it may be possible to define antitargets such as KIT in the case of AML to allow improved kinase inhibitor design of clinical agents with enhanced efficacy and reduced toxicity.

Introduction

Kinase inhibitors are among the fastest growing new class of therapeutics for treating cancer, with 25 new kinase inhibitors approved by the FDA in the last 14 years.[1] Since these agents almost exclusively target a kinase's highly conserved ATP binding pocket, selectivity is problematic. A limiting feature of kinase inhibitors is that their ability to target multiple wild-type kinases in normal tissues limits the doses that can be used to target the mutant kinase in the tumor tissue. The key question, in light of the complex kinase networks in all cells, is which anti-targets should be avoided, in order to limit toxicity in normal tissues. Our work[2,3] and that of others,[4,5] has highlighted the potent effects of multi-targeted kinase inhibitors, revealing unexpected effects when several kinases are inhibited rather than each one individually (synthetic lethal effects as well as positive epistatic effects). By understanding the synthetic lethal effects on normal cells and developing selective inhibitors which avoid even a small number of "off-target" kinases, we believe clinical agents with an improved therapeutic index can be developed.

One disease where this anti-target[2] concept is particularly needed is AML, a rapidly fatal blood cancer comprising 2% of cancer deaths in the United States in 2013 and a disproportionate number of new cases (ca. 19,000, 30%) and deaths (ca. 10,500, 44%) relative to all leukemias.[6] FDA-approved chemotherapy has not advanced beyond general cytotoxic agents, and no highly active therapies have been approved in over 30 years. The cure-rate for AML remains approximately 25%. Fms-Like Tyrosine Kinase 3 (FLT3) is a receptor tyrosine kinase (RTK) regulating hematopoietic differentiation that is mutated in 30 – 35% of AML cases, making it the most frequently mutated gene in AML.[7] 25% of AML patients present with juxtamembrane (JM) domain duplications termed *I*nternal *T*andem *D*uplications (FLT3-ITD).[8] The ITD mutation is thought to

render FLT3 constitutively active by disrupting an autoinhibitory function of the JM domain. Patients with FLT3-ITD mutations have significantly increased relapse rates and shortened survival, thus illustrating a major unmet therapeutic need.

FLT3-ITD was recently validated as a therapeutic target in AML.[9] Several targeted FLT3 tyrosine kinase inhibitors (TKIs) have been investigated, however none have advanced beyond Phase III clinical trials.[10] The FLT3 TKI AC220 (Quizartinib)[11] achieves substantial reduction in leukemic blasts initially in a high proportion of patients, and is the most kinome-wide selective clinical candidate.[12] However, in spite of its promising selectivity, which is remarkably confined to inhibition of the Class III/PDGFR family of RTK's, AC220-induced myelosuppression represents a major dose-limiting toxicity.[13,14] As a result, while many patients achieve clearance of bone marrow (BM) blasts, most experience incomplete recovery of normal blood counts (CRi) and remain at risk of complications such as life-threatening infection or bleeding.

The Class III family of RTKs (comprising FLT3, KIT, CSF1R, PDGFRα, and PDGFRβ) are important regulators of normal hematopoiesis. In 1995, Lemischka and coworkers showed that mice lacking function of either Flt3 or Kit maintained overall normal populations.[15] However, mice lacking both Flt3 and Kit function had a dramatic reduction of hematopoietic cell numbers, ca. 15-fold white cell depletion, reduction of lymphoid progenitors and postnatal lethality. We propose that KIT is an anti-target[2] in the context of pharmacologic inhibition of FLT3. Thus, normal mature hematopoietic populations can be maintained in the context of either Flt3 or Kit inhibition alone, but not dual Flt3/Kit inhibition.[16]

This synthetic lethal toxicity relationship between FLT3 and KIT for maintaining normal hematopoietic populations may explain the adverse side effects of the current kinase targeted drugs in clinical development. In a recent single agent Phase II trial, PKC412 failed to achieve a single complete remission (CR). When combined with cytotoxic agents PKC412 showed some promise, achieving a 25% CR rate, but responses were primarily incomplete recovery of peripheral blood counts (CRi, 20%) with over 90% of patients developing grade 3/4 myelosuppression.[17] While AC220 monotherapy impressively demonstrated a 50% CR rate in a Phase II trial, these consisted primarily of CRi (45%) with few real CRs with complete recovery of blood counts,[18] correlating with the similar potency of these agents for both FLT3 and KIT. A recent study showed increased selectivity of the clinical agent crenolanib for FLT3 over KIT and reinforced the correlation between target inhibition, and anti-target avoidance,[2] which lead to lowered toxicity towards normal hematopoiesis.[19] However, the potency of crenolanib for KIT remains too high (IC_{50} = 67 nM for p-KIT inhibition in TF-1 cells; 65% inhibition at 100 nM, in vitro).[19] This is likely insufficient to fully minimize clinically relevant myelosuppression, as a recent interim analysis reported only a 17% (3/18 patients) composite CR rate in AML patients, with 2/3 of these responders achieving only CRi.[20] These findings highlight the need for new clinical candidates that better minimize KIT and other Class III RTK inhibition.

While avoiding inhibition of the presumed anti-target, KIT, is one chemical challenge toward inhibitor design, the emergence of on-target resistance is another clinical challenge. We[9] and others[21] have identified the acquisition of secondary FLT3 KD mutations that cause drug resistance as another limitation of current clinically active

FLT3 inhibitors. Mutations at the activation loop residue D835 are particularly clinically problematic. These mutations are proposed to bias the kinase toward the constitutively *active* conformation by disrupting a hydrogen bond from D835 to S838, and thus limit the efficacy of Type II inhibitors such as AC220. We have recently proposed that a Type I inhibitor, which binds to the active kinase conformation, would circumvent these mutations that confer resistance to AC220.[9] New small molecule therapies have been reported to bypass these particular mutations, including crenolanib,[19] a Type I inhibitor, [22,23] but the CR rate of crenolanib remains modest.[20] Moreover, it is likely that a repertoire of drugs will be necessary to combat emerging resistance.

We propose herein a solution to the FLT3/KIT selectivity problem designed to avoid myelosuppression and also retain potency against drug resistant mutations. The staurosporine scaffold has been utilized pharmacologically for 30 years and staurosporine analogs have been proven to be potent FLT3 inhibitors (PKC412, CEP701),[17] though clinical activity of these compounds has been modest, perhaps caused by lack of potent FLT3 inhibition due to dose-limiting toxicity in vivo. The lactam ring C7 position remains virtually unexplored for modulating selectivity.[24,25,26] We recently reported that C7-substituted staurosporine analogs, we term "staralogs", are potent and selective inhibitors of engineered analog-sensitive (AS) kinases.[27] For example, when C7 (R_1) equals isobutyl (Star 12), AS Src kinase is potently inhibited but WT kinases remain unaffected. However, we also observed that Star 12, in a panel of 319 kinases, weakly inhibits only one WT kinase, FLT3 (57% inhibition at 1μM; KIT, CSF1R, PDGFRα/β all inhibited <10%). Thus, the C7-alkyl group of Star 12 may allow for weak but selective inhibition of FLT3 over the anti-target KIT, which contributes to myelosuppression when

FLT3 is also inhibited. Although substitution of an isobutyl group at C7 reduced potency, we hypothesized that combining the FLT3/KIT selectivity of Star 12 and the potency features of PKC412 would generate an optimal FLT3 inhibitor also capable of targeting emerging mutations (**Figure 1A**).

Results:

Discovery and in vitro structure activity relationships (SAR) towards Star 27, a FLT3/KIT selective drug

In an effort to identify an optimal C7 substituent that retains selectivity away from KIT while enhancing potency for FLT3, we synthesized and tested a panel of C7-substituted staralogs (**Figure 1B**). The C7 substituent points toward the gatekeeper residue of the kinase,[27] and FLT3 and KIT possess Phe and Thr gatekeepers, respectively. We chose an unbiased selection of groups easily derived from the chiral pool, and tested these derivatives in a radiolabeled purified kinase assay, finding that the alanine-derived methyl group provided the most potent inhibition. Synthesis of C7 analogs was further expedited by testing the fully aglyconic derivatives (see **Figure 1B**, entries 1 – 8). Replacement of the sugar moiety of PKC412 with a pendant amine has proven to be a means to reduce the chemical synthetic burden of carbohydrate synthesis while simultaneously maintaining potency. Attachment of *n*-propyl amine to mimic the *N*-methyl amide of PKC412 produced comparable values (**Figure 1B**, Star 27: 1.5 nM; PKC412: 2 nM). Interestingly, both Star 27's one carbon homolog (Star 23) and regioisomer (Star 27-*iso*) reduced activity, further indicating a well-defined structure activity relationship (**Figure 1B**).

We next evaluated our lead inhibitors to show the role of C7 modification on the ratio of KIT/FLT3 IC_{50}'s. While PKC412 exhibited potent inhibition of all five Class III RTKs (**Figure 1C**, IC_{50} = <0.5 – 36 nM), Star 23 showed improved differentiation between FLT3 and other Class III RTKs (IC_{50} = 9 – >10,000 nM), and Star 27 proved to have the best selectivity (IC_{50} = <0.6 – 9,880 nM). This selectivity increases from a) KIT/FLT3 ratio of >72 for PKC412 to >1,700 for Star 27 and b) CSF1R/FLT3 ratio of 8 for PKC412 to >16,500 for Star 27 (**Figure 1C**). Correlation is seen with inhibition of kinases containing Phe gatekeepers (GKs) and avoidance of those containing Thr GKs, for C7-Me containing staralogs.

We then profiled Star 27 against 319 purified kinases using the same assay conditions used previously for PKC412. We chose to screen for additional targets at 1μM, or 1,000-fold above the IC_{50} value for the desired target, which captures the maximum number of targets of each inhibitor, dendrograms showing in **Figures 1D** (PKC412) and **1E** (Star 27). At this high concentration the two drugs inhibit many of the same targets. Yet, importantly, the two drugs show important differences in the tyrosine kinase family. The percent inhibition of 54 Tyr kinases by Star 27 with respect to their percent inhibition by PKC412 is shown in **Figure 1F**. This plot indicates a substantial shift towards inhibition by PKC412 but not Star 27 and correlates with a high number of Thr GK residues (42 Thr GKs for Tyr kinases vs 34 Thr GKs in non-Tyr kinases). This shift is particularly striking for the entire Src family (**Figure 1D**, pink triangles), all members of which possess Thr GKs. Conversely, Tyr kinases that possess Phe GKs mostly display high and equipotent inhibition by both Star 27 and PKC412 (including FLT3, TRKA, TRKB, and TRKC).

Star 27 demonstrates increased selectivity for FLT3 over KIT in cellular models

We compared PKC412 to Star 27 for the ability of each to inhibit cell proliferation of human cell lines addicted to FLT3 or KIT. We employed Molm14 and MV4;11 cells, harboring the FLT3-ITD mutation (hetero- and homozygous, respectively); HMC1.1 cells (dependent on KIT V560G); and K562 cells (which express the BCR-ABL fusion kinase) as a control for non-KIT-related toxicity. Sorafenib, AC220, and ponatinib all displayed equipotent inhibition of FLT3 and KIT-driven cell lines (see **Figure 2A** and reference values[28,29,32]). PKC412 increases this selectivity 22 fold (HMC1.1/MV4;11). Encouragingly, Star 27 inhibited proliferation of the FLT3-ITD+ cells while not affecting HMC1.1 proliferation leading to a selectivity window of >122-fold (HMC1.1/MV4;11).

We next tested if this inhibition of proliferation was manifest in triggering apoptotic cell death. Analysis of caspase-3 activation revealed a similar induction of apoptosis in a dose-response manner between PKC412 and Star 27 in Molm14 cells (**Figure 2B**). Conversely, PKC412 induced apoptosis in the KIT mutant HMC1.1 cells as predicted while minimal apoptosis was observed for Star 27, further highlighting the selectivity of Star 27 for FLT3 over KIT (**Figure 2C**).

Given the similarity in potency between PKC412 and Star 27 towards FLT3, we next tested both compounds for their ability to inhibit FLT3 autophosphorylation as well as downstream signaling in Molm14 cells. We observe a similar inhibition of p-FLT3 inhibition between the two drugs and downstream phosphorylation among three canonical signaling arms was uniform between PKC412 and Star 27 (JAK/STAT,

RAS/ERK, and mTOR/AKT/S6; **Figure 2D**). In contrast to similar phospho-signaling inhibitory profiles in Molm14 cells, PKC412 inhibited p-KIT and downstream signaling to a greater degree in HMC1.1 cells compared to Star 27 (**Figure 2D**).

PKC412 but not Star 27 exhibited myeloid toxicity in an ex vivo model of human hematopoiesis while both inhibited primary AML blast colony formation

We next asked if FLT3/KIT selectivity could maintain efficacy and reduce toxicity in primary patient-derived contexts. Colony-forming assays are useful for this application because they better represent the microenvironment of the BM niche than traditional cell proliferation of primary human cells.[30] Testing both PKC412 and Star 27 demonstrated their ability to inhibit the growth of primary patient-derived FLT3-ITD+ blasts in colony forming assays, with both demonstrating >80% inhibition of colony formation at 1,000 nM (**Figures 3A,B**). Because of the importance of maintaining potency against kinase domain (KD) mutations in addition to those of the JM domain, we also tested the ability of both drugs to inhibit the colony-forming ability of primary patient blasts containing a FLT3-D835 mutation (ITD–; point mutational status undetermined). Star 27 inhibited about 60% of colonies at 1,000 nM while PKC inhibited about 80% (**Figure 3C**).

Alternatively, we tested PKC412 and Star 27 for their effects on hematopoietic colony formation of normal BM and stimulated peripheral blood (SPB) samples. One of the four donor samples is shown in **Figure 3D**. **Figures 3E,F** show quantification of colony counts for both erythroid (or burst) forming units (BFUs) and colony forming units (CFUs). PKC412 demonstrated dose-dependent inhibition of colony formation from

normal hematopoetic progenitors while Star 27 demonstrated no significant effect up to a concentration of 1,000 nM (**Figures 3E,F**).

In vivo zebra fish model shows Star 27 to be non-myelosuppressive, PKC412 to be myelosuppressive, and both drugs to be efficacious against FLT3-ITD AML

Having validated Star 27's biochemical potency and lack of myelosuppression, we next tested its effects in vivo. We chose the established model, *D. rerio* (zebrafish) for studying hematopoiesis[31,32]. In this model, cells transduced with FLT3-ITD and treated with AC220 have been shown to recapitulate knock-down of FLT3-ITD in clinical studies[33]. This model also provides for robust and sensitive measures of in vivo myelopoiesis.[33]

We treated embryos with Star 27 up to 10 μM and studied the effects on WT morphology at 3 days post fertilization (dpf), finding no change in heart and tail morphology (tail length and lack of curvature, see **Figures 4A-D**). In contrast, PKC412 showed substantial morphological defects to the heart at 1 μM vs vehicle, **Figures 4E-I**), tail length and tail curvature at 1 μM and 2.5 μM (see **Figures 4E**, and **4G**, respectively).

We next examined the effect of Star 27 and PKC412 on WT granulopoiesis as a measure of KIT-related myelopoiesis/myelosuppression measured by myeloperoxidase-(mpx) stained in situ hybridization in the posterior blood island (PBI). Representative cross sections for the PBI for DMSO, Star 27, and PKC412 are shown (**Figures 4J**, **4K**, **and 4L**, respectively). Quantification of mpo dots in Star 27 treated embryos shows a non-significant difference between 10 μM and DMSO treatments of 30 hours post

fertilization (hpf, **Figures 4J**,**K**,**M**). In contrast, PKC412 showed statistically significant suppression of myelopoiesis at 10 μM (**Figure 4M**).

Efficacy in the AML FLT3-ITD context is quantified by binning the FLT3-ITD blast phenotype into Normal, Intermediate and Severe states (**Figures 4N-P**, respectively).[33] Star 27 did have efficacy in preventing the spread of neutrophilic blasts in FLT3-ITD-transduced embryos (**Figure 4Q**) similar to that previously seen with AC220.[33] Similar to Star 27, PKC412 also showed an ability to limit the spread of FLT3-ITD-injected leukemic blasts (**Figure 4Q**).

Calculation predicts selectivity for Star 27 based on electronics and may be general beyond Class III RTKs

The structural basis of selectivity of Star 27 for FLT3 over other Class III RTKs was computationally investigated, revealing two features of staralog binding that may explain Star 27's selectivity for FLT3 over KIT, versus PKC412's equipotency towards both kinases. (a) Electronics: we calculate that PKC412 maintains a partial positive charge at its lactam C7 position, matching the partial negative charge of KIT's Thr GK (**Figures 5A-C**), while Star 27's C7 methyl renders its lactam relatively neutral (**Figures 5D-F**), reducing this affinity interaction. (b) Sterics: staralogs with no C7 substitution maintain a flat lactam for binding to the hinge region, adjacent to the gatekeeper. Based on crystallographic data from KIT's active conformation,[34] a simple steric argument may explain why Star 27's C7 methyl group prevents binding to KIT's restricted ATP binding pocket while PKC412 potently binds (data not shown). Conversely, FLT3's active site is hypothetically large enough to accommodate the 17.4 $Å^3$ van der Waal's volume of

methyl (vs. 1.17 $Å^3$ for H). Taken together both arguments may explain the greater affinity of PKC412 for both kinases and of Star 27 for FLT3 but not KIT (calculated using MOE ver2013.0801). Taken together, this model may account for the selectivity seen for Star 27 for kinases bearing Phe GKs (FLT3, TRK, etc.) and away from those bearing Thr GKs (KIT, CSF1R, Src family, other Tyr kinases, see **Figure 1D**).

Star 27 shows uniform potency against drug-resistant mutant cell line proliferation

Mutations that confer drug resistance to existing Type II FLT3 inhibitors AC220 and sorafenib commonly prevent the kinase from efficiently adopting an inactive conformation required for drug binding. Type I FLT3 inhibitors, such as PKC412 and Star 27, are predicted to be less vulnerable to such mutations. We tested both inhibitors against a panel of 17 cell lines containing different FLT3 TKI mutations with varying resistance to the leading clinical candidate therapies, sorafenib, ponatinib, and AC220 (**Figure 6A**). IC_{50} values are presented as $\log_{10}$-fold resistance in a color-coded heat map to highlight the range of offset. Using published IC_{50} values for sorafenib, AC220, and ponatinib for comparison,[28,29,35] we observed equipotent values for PKC412 against most KD point mutants. Intriguingly, Star 27 maintained similar potency against most mutants compared to FLT3-ITD alone.

Crenolanib is a potent inhibitor of p-KIT and normal BM colony formation

Crenolanib has been reported to inhibit p-KIT in TF-1[19] cells and HMC1.2[23] cells at 67 nM and <100 nM IC_{50}'s, respectively. In order to directly compare to our results with PKC412 and Star 27 (**Figure 2D**), we tested crenolanib's biochemical inhibition of

298 p-KIT in HMC1.1 cells. **Figure 6B** shows crenolanib inhibits p-KIT in these cells at an
299 IC_{50} of 12 nM. This potency against KIT anti-target is propagated down to inhibition of
300 p-AKT and p-S6 kinases. Crenolanib's potency against p-FLT3 has been reported to be 5
301 nM.[19]

302 Crenolanib has been reported to have only modest inhibition of normal BM
303 colony formation of CFUs and no inhibition of BFUs up to 200 nM drug treatment.[19]
304 However, the lack of both higher drug dosing (>200 nM) and statistically comparable
305 variation prompted us to retest crenolanib in the same colony forming assay up to 1,000
306 nM, to compare to PKC412 and Star 27 (**Figure 3D-F**). We observe crenolanib to have a
307 more substantial dampening of normal colony growth of both CFU and BFU subtypes in
308 normal BM (see **Figure 6C**).

309

310 **Discussion:**

311 The aggressive nature of FLT3-driven AML and the lack of effective and well-
312 tolerated targeted therapy represents a major unmet therapeutic need. Currently, the most
313 promising clinical targeting agents cause myelosuppression in most patients regardless of
314 remission status. As kinase inhibitor based therapies evolve, refined selectivity against
315 particular off-targets (so-called anti-targets[2]) will drive chemical design.[36] Avoiding
316 specific anti-targets will hopefully lead to a reduction in dose-limiting toxicities that will
317 allow more complete inhibition of the oncogenic drivers of disease.

318 A former targeted clinical candidate, tandutinib (MLN518), may further
319 demonstrate directly the affects of the FLT3/KIT synthetic lethal toxicity model.[37]
320 MLN518 was indicated to have similar IC_{50}'s for FLT3 and KIT phosphorylation (220

and 170 nM, respectively). While MLN518 showed promise with reducing FLT3-ITD+ blasts in primary patient-derived samples, exposure of the drug to the BM of healthy individuals at a dose necessary for primary FLT3-ITD+ CFU reduction, led to severe depletion of healthy hematopoietic colony formation at 1 μM.

The most direct evidence exists for FLT3/KIT as a synthetic lethal toxic pair, however, other Class III RTKs may exhibit synthetic lethal effects in terms of dose-limiting toxicity when treating FLT3-driven disease. Another Class III RTK, CSF1R, has been shown via the knockout "toothless" rat model (tl = $csf1r^{-/-}$) to be important to osteoclastogenesis,[38] colon development,[39] and for normal macrophage and dendritic cell (DC) production and maintenance.[40] Perhaps most importantly, tl rats have been reported with a 32% platelet loss, and this thrombocytopenia was not reversed by BM transplant.[41] Star 27 exhibits a large selectivity window with a >16,500/1 CSF1R/FLT3 IC_{50} ratio (**Figure 1C**), which may provide a clinical benefit. However, more work is needed to determine the synthetic lethal toxicity of CSF1R since other reports suggest an opposite and more complicated role for it in hematopoiesis.[42]

Our focus on the staurasporine scaffold maintains the beneficial aspects of PKC412's potency against drug-resistant FLT3 mutations (**Figure 6A**). Since both staralogs are Type I inhibitors they are not expected to suffer from the Type II-resistance model at the gatekeeper (F691L) and especially activation loop (D835) mutations observed in the clinic.[9] The reduced potency of Star 27 against FLT3 relative to PKC412 in Ba/F3 cells (**Figure 6A**) is mitigated by the more relevant comparison in human cells (**Figure 2A**) as well as the predicted increase in maximum tolerated dosing for clinical candidates avoiding the KIT anti-target. Robustness against emergent mutations is a

desirable feature of PKC412 but its pan-Class III RTK inhibition (especially KIT) is likely a major limitation addressed here. Remarkably, the addition of a single methyl group (CH_3) likely caused the observed decrease in toxicity.

The strategy reported here for gaining selectivity for FLT3 inhibition over KIT and other Class III RTKs may have importance in other hematopoietic pathology as well. FLT3 has been shown to be important for classical DC maintenance and necessary for inflammatory DCs.[43] Consequently, FLT3 has been proposed to be a drug target for autoimmunity and inflammation, particularly atherosclerosis. The staralog, CEP701, has been investigated in this context but it is expected that its promiscuity, particularly among KIT and CSF1R, will hamper clinical development.[42] Star 27 should enable a reduction in FLT3-associated inflammation and autoimmunity while allowing KIT and CSF1R to compensate with classical DC maintenance. Furthermore, the generality of our electrostatic Phe GK inhibition coupled with Thr GK avoidance model (**Figure 1D,5**) may guide future medicinal chemistry efforts, while our in vivo study shows any promiscuity seen in **Figure 1E** does not compromise Star 27's efficaciousness in a well-validated in vivo model of hematopoiesis.[31,32,33]

Recent clinical experience with targeted inhibition of mutated kinases in cancer suggests that efficacy is driven by maximal pathway inhibition. In the case of vemurafenib, <80% pathway inhibition in BRAF (V600E) mutant melanoma afforded no tumor shrinkage, while >90% inhibition showed profound clinical benefit.[44] The challenge is that inhibitors of the oncogene also exhibit off-target effects on closely related kinases that inevitably lead to dose limiting toxicities. The goal of advancing improved molecular targeted therapies is to identify the key anti-targets that drive toxicity

and develop agents that avoid these effects. Our work highlights the synthetic lethal toxicity of an anti-target (KIT) when the oncogenic kinase (FLT3) is inhibited. As more complete understanding of kinase networks emerge it may be possible to delineate the anti-targets to avoid in numerous disease settings to allow improved kinase inhibitor design that can lead to greater ability to inhibit the disease causing pathway activation while avoiding systemic toxicities.

Methods

Inhibitors. PKC412 was purchased from Selleckchem.

Chemical synthesis. Staralogs (**Figure 1B**) were synthesized according to precedent.[27] This protocol was adapted for synthesis of Star 27. Materials obtained commercially were reagent grade and were used without further purification. 1H NMR and 13C NMR spectra were recorded on Varian 400 or Brucker 500 spectrometers at 400 and 125 MHz, respectively. Low resolution mass spectra (LC/ESI-MS) were recorded on a Waters Micromass ZQ equipped with a Waters 2695 Separations Module and a XTerra MS C18 3.5 mm column (Waters). Reactions were monitored by thin layer chromatography (TLC), using Merck silica gel 60 F254 glass plates (0.25 mm thick). Flash chromatography was conducted with Merck silica gel 60 (230−400 mesh).

In Vitro Kinase Assays. For **Figure 1B** purified FLT3 WT was diluted in kinase reaction buffer (10mM HEPES [pH 7.6], 10 mM $MgCl_2$, 0.2 mM DTT, 1mg/mL BSA) to

a concentration of 2 nM and pre-incubated with 2.5% (v/v) DMSO, 100 μM peptide (sequence EAIYAAPFKKK (Abltide)), and varying concentrations of inhibitor from 20 μM by fourths down to 1.2 nM for 10 min pre-incubation. Kinase reactions were initiated by the addition of 100 μM cold ATP supplemented with 2.5 μCi γ32P ATP per well and allowed to proceed at RT. At 15 minutes 3 μL of the reactions were spotted onto phosphocellulose sheets (P81, Whatman) and subsequently soaked in wash buffer (1.0% (v/v) phosphoric acid) at least 5 times for 5 minutes each. The sheets were then dried, and transferred radioactivity was measured by phosphorimaging using a Typhoon scanner (Molecular Dynamics). Radioactive counts were quantified using ImageQuant software, and titration data were fit to a sigmoidal dose response to derive IC50 values using the Prism 4.0 software package. Experiments were performed 2-4 times, each in triplicate, with eight dosages, to derive standard error of the mean values. For **Figure 1C**, values obtained at Reaction Biology Corporation. Briefly, specific kinase/substrate pairs were prepared in reaction buffer; 20 mM Hepes pH 7.5, 10 mM $MgCl_2$, 1 mM EGTA, 0.02% Brij35, 0.02 mg/mL BSA, 0.1 mM Na3VO4, 2 mM DTT, 1% DMSO. Compounds were delivered into the reaction, followed 20 min later by addition of a mixture of ATP (Sigma) and 33P ATP (PerkinElmer) to a final concentration approximating each kinase's $K_{m\text{-}ATP}$ (FLT3: 50 μM; KIT: 150 μM; CSF1R: 150 μM; PDGFRa: 5 μM; PDGFRb: 50 μM). Reactions were carried out at 25 °C for 120 min, followed by spotting of the reactions onto P81 ion exchange filter paper (Whatman). Unbound phosphate was removed by extensive washing of filters in 0.75% phosphoric acid. After subtraction of background derived from control reactions containing inactive enzyme, kinase activity data were expressed as the percent remaining kinase activity in test samples compared to

vehicle (dimethyl sulfoxide) reactions. IC_{50} values and curve fits were obtained using Prism (GraphPad Software). Data obtained in singlicate with two biological replicates and IC_{50} values presented ± SEM in **Figure 1C**.

Kinome Profiling. 319 kinases were tested in a duplicate single dose (1 μM) format using a ^{33}P-labelled ATP activity assay performed by Reaction Biology Corp. Assays performed at identical conditions to those of PKC412.[45]

Cell Lines. Stable Ba/F3 lines were generated by retroviral spinfection with the appropriate mutated plasmid as previously described.[9]

Cell-Viability Assay. Exponentially growing cells (5×10^3 cells per well) were plated in each well of a 96-well plate with 0.1 mL of RPMI 1640+10% (vol/vol) FCS containing the appropriate concentration of drug in triplicate, and cell viability was assessed after 48 h as previously described.[9] Log_{10} fold selectivity heat maps for **Figures 1C, 7**: Briefly, IC50 values were calculated as shown in figures, then ratios of RTK/FLT3 (**Figure 1C**) or point mutant/BaF3 FLT3 ITD (**Figure 7**) calculated. Log10-scale transformation of ratios, followed by conditional formatting using xcel spreadsheet software yielded the colored diagrams shown.

Assessment of Caspase-3 Activation. Exponentially growing cells were plated in the presence of PKC412 or Star 27 in RPMI+10% (vol/vol) FCS for 48 h. Cells were fixed with 4 % (vol/vol) paraformaldehyde (Electron Microscopy Sciences) and permeabilized

with 100% (vol/vol) methanol (Electron Microscopy Sciences) followed by staining with a FITC-conjugated antiactive caspase-3 antibody (BD Pharmingen). Cells were run on a BD LSRFortessa cell analyzer, and data were analyzed using FlowJo (Tree Star Inc.). Percentage of live cells was determined by negative staining for activated caspase-3 (see **Figures 2B,C**).

Immunoblotting. Exponentially growing Molm14, HB119, or Ba/F3 cells stably expressing mutant isoforms were plated in RPMI medium 1640+10% (vol/vol) FCS supplemented with PKC412 or Star 27 at the indicated concentration. HMC1.2 cells were cultured and treated in IMDM + 10% FCS. After a 90 min incubation, the cells were washed in PBS, lysed, and processed as previously described. Immunoblotting was performed using anti-phospho-FLT3, anti-phospho-KIT, anti-phosphoSTAT5, anti STAT5, anti-phosphoERK, antiERK, anti-phosphoS6, anti-S6, antiKIT (Cell Signalling) and anti-FLT3 S18 antibody (Santa Cruz Biotechnology).

Zebrafish maintenance and embryo collection. Wild-type (WT) zebrafish were maintained under standard conditions and embryos were staged as described.[33] The study was approved by the Committee of the Use of Live Animals for Teaching and Research in The University of Hong Kong.

Assessment of FLT3 Colony Assays in Primary Patient Blasts. Primary AML blood samples and/or marrow aspirates were obtained on an IRB-approved protocol at the University of California, San Francisco. Informed consent was obtained in accordance

with the Declaration of Helsinki. Mononuclear cells were purified by density centrifugation (Ficoll-Paque Plus, GE Healthsciences) before cryopreservation in 10% (vol/vol) DMSO or FCS (primary ITD and D835-mutant assays, **Figures 3A-C**) or immediate use in assays (Normal BM and SPB, **Figsures 3D-F**). Normal BM and stimulated peripheral blood (SPB) samples were collected from donors at the UCSF oncology/hematology division. Cells were then suspended in MethoCult methylcellulose (Stem Cell Technologies, product no. H4435 Enriched) in 15 mL Falcon tubes, vigorously vortexed, bubbles settled over 10 minutes. Triplicates then plated via blunt-nosed syringe (1.1 mL each) into 3 cm dishes, avoiding bubble generation, and each dish placed in a larger 10 cm dish with water trough in an incubator (37^{o}C, 5% CO_2) for 13-14 days. Colonies were counted individually using traditional microscopy. CFU and BFU types reported separately (CFU-GEMM colonies counted as one of each). Results shown for FLT3 ITD primary blasts (**Figure 3E**) are a combination of leukemic blast colonies and BFU colonies.

Generation of Mutants. Mutations isolated in the screen were engineered into pMSCVpuroFLT3–ITD by QuikChange mutagenesis (Stratagene) as previously described.[9]

Acknowledgements

We gratefully acknowledge the Howard Hughes Medical Institute (K.M.S.), the Leukemia and Lymphoma Society (C.C.S., E.A.L., K.L., N.P.S.), the National Institute of Health (NIHGMS R012R01EB001987, 1R01GM107671-01) (KMS), and the Waxman

Foundation (K.M.S.). We thank Dr. Masanori Okaniwa for assistance with modeling studies (**Figure 5**), and Evan Massi for **Figure 6B**.

Author Contributions

A.W. and M.L. designed and synthesized staralog compounds and designed purified kinase assays with staralogs and A.W. tested staralogs in vitro. C.S., A.W. and K.L. designed cellular proliferation assays and K.L. and A.W. performed assays. A.W. and E.L. designed apoptosis and biochemical assays and E.L. performed assays. A.W. and C.S. designed normal and malignant bone marrow colony assays and A.W. performed assays. A.W., B.-L.H., and A.Y.H.L. designed zebrafish studies, B.-L.H. performed studies, and A.W., B.-L.H. and A.Y.H.L. analyzed data. A.W., C.S., M.L., E.L., N.S., and K.S. analyzed data and A.W. and K.S. wrote the paper with input from all authors.

Corresponding authors. Kevan M. Shokat (kevan.shokat@ucsf.edu), Neil P. Shah (nshah@medicine.ucsf.edu), Catherine C. Smith (csmith@medicine.ucsf.edu).

[1] Mullard, A. 2013 FDA drug approvals *Nature Reviews Drug Discovery* **13,** 85–89 (2014)
[2] Dar, A.C., Das, T.K., Shokat, K.M. & Cagan, R.L. Chemical Genetic Discovery of Targets and Anti-targets for Cancer Polypharmacology *Nature* **486**, 80–85, (2012).
[3] Kung, C., Kenski, D.M., Krukenberg, K., Madhani, H.D., Shokat, K.M., Selective Kinase Inhibition by Exploiting Differential Pathway Sensitivity *Chem. Biol.* **13**, 399–407, (2006).
[4] Wilhelm, S. et al. Discovery and development of sorafenib: a multikinase inhibitor for treating cancer. *Nature Rev. Drug Discov.* **5**, 835–844 (2006).
[5] Ahmad, T. & Eisen, T. Kinase inhibition with BAY 43-9006 in renal cell carcinoma. *Clin. Cancer Res.* **10**, 6388S–6392S (2004).
[6] Leukemia and Lymphoma Society *Facts 2014* http://www.lls.org/content/nationalcontent/resourcecenter/freeeducationmaterials/generalcancer/pdf/facts.pdf
[7] Mizuki, M., *et al.* Flt3 mutations from patients with acute myeloid leukemia induce transformation of 32D cells mediated by the Ras and STAT5 pathways *Blood* **96**, 3907–3914, (2000).
[8] Kindler, T., *et al.* Identification of a Novel Activating Mutation (Y842C) within the Activation Loop of FLT3 in Patients with Acute Myeloid Leukemia (AML) *Blood* **105**, 335–340, (2005).

[9] Smith, C.C., *et al.* Validation of ITD Mutations in FLT3 as a Therapeutic Target in Human Acute Myeloid Leukemia *Nature* **485**, 260–263, (2012).
[10] Smith C.C. & Shah N.P. The role of kinase inhibitors in the treatment of patients with acute myeloid leukemia. *Am. Soc. Clin. Oncol. Educ. Book* 313. doi: 10.1200/EdBook_AM.2013.33.313, (2013).
[11] Chao, Q., *et al.* "Identification of N-(5-tert-Butyl-isoxazol-3-yl)-N'-{4-[7-(2-morpholin-4-yl-ethoxy)imidazo[2,1-b][1,3]benzothiazol-2-yl]phenyl}urea Dihydrochloride (AC220), a Uniquely Potent, Selective, and Efficacious FMS-Like Tyrosine Kinase-3 (FLT3) Inhibitor". *J. Med. Chem.* **52**, 7808–7816, (2009).
[12] Zarrinkar, *et al.* AC220 is a uniquely potent and selective inhibitor of FLT3 for the treatment of acute myeloid leukemia (AML). *Blood.* **114**, 2984–2992, (2009).
[13] Smith, C.C.; Shah, N.; *unpublished results*
[14] Galanis, A, *et al.* Crenolanib: A next generation FLT3 inhibitor *Am. Soc. Hem.* Abstract no. 3660. (2011).
[15] Mackarehtschian, K. *et al.* Targeted Disruption of the flk2/flt3 Gene Leads to Deficiencies in Primitive Hematopoietic Progenitors *Immunity* **3**, 147–161, (1995).
[16] For examples and definition of "negative epistasis", (this particular type of synthetic lethality/toxicity), see: Bershtein, S., Segal, M., Bekerman, R, Tokuriki, N. & Tawfik, D.S. Robustness–epistasis link shapes the fitness landscape of a randomly drifting protein *Nature* **444**, 929–932, (2006).
[17] Stratl, P.; *et al.* "Early Results of a Phase I/II Trial of Midostaurin (PKC412) and 5-Azacytidine (5-AZA) for Patients (Pts) with Acute Myeloid Leukemia and Myelodysplastic Syndrome *Blood* **122** 3949, (2013).
[18] Cortes, J. E., *et al.* Results of a Phase 2 Randomized, Open Label, Study of Lower Does of Quizartinib (AC220; ASP2689) in Subjects with FLT3-ITD Positive Relapsed or Refractory Acute Myeloid Leukemia (AML) *Blood* **122** 494, (2013).
[19] Galanis, A. *et al.* Crenolanib is a potent inhibitor of FLT3 with activity against resistance-conferring point mutants *Blood* **123** 94–100, (2014).
[20] Collins, R. *et al.* Clinical activity of crenolanib in patients with D835-mutant FLT3-positive relapsed/refractory acute myeloid leukemia (AML) *2014 ASCO National Meeting Ab. No. 7027* (2014).
[21] Wodicka, L. M. et al. Activation state-dependent binding of small molecule kinase inhibitors: structural insights from biochemistry. *Chem. Biol.* **17**, 1241–1249 (2010).
[22] Lee H.K., *et al.* G-749, a novel FLT3 kinase inhibitor can overcome drug resistance for the treatment of Acute Myeloid Leukemia. *Blood* **123**, 2209–2219, (2014).
[23] Smith C. C., *et al.* Crenolanib is a selective type I pan-FLT3 inhibitor *Proc. Natl. Acad. Sci. USA* **111**, 5319–5324, (2014)
[24] The N676X mutation has been found in one patient and IC50 differences for this point mutant vs. FLT3 ITD are small (*unpublished results*) possibly due to PKC412's high protein binding, leading to a low barrier of resistance. See Heidel F., *et al.* Clinical resistance to the kinase inhibitor PKC412 in acute myeloid leukemia by mutation of Asn-676 in the FLT3 tyrosine kinase domain. *Blood* **107**, 293–300, (2005).
[25] Bishop, A. C., *et al.* A Chemical Switch for Inhibitor-Sensitive Alleles of any Protein Kinase *Nature* **407**, 395−401, (2000).
[26] Wood, J.L., Petsch, D.T., Stoltz, B.M. & Hawkins, E.M. Total synthesis and protein kinase activity of C(7) methyl derivatives of K252a *Synthesis*, **1**, 1529−1533, (1999).
[27] Lopez M.S., *et al.* Staurosporine-derived inhibitors broaden the scope of analog-sensitive kinase technology. *J Am Chem Soc.* **135**, 18153–18159, (2013).
[28] Guo, T. *et al.* Sorafenib Inhibits the Imatinib-Resistant KIT^{T670I} Gatekeeper Mutation in Gastrointestinal Stromal Tumor *Clin. Cancer Res.* **13**, 4874–4881, (2007).
[29] Kampa-Shittenhelm, K.M., *et al.* Quitartinib (AC220) is a potent second generation class III tyrosine kinase inhibitor that displays a distinct inhibition profile against mutant *FLT3, -PDGFRA* and *–KIT* isoforms *Molecular Cancer* **12**, 1–15, (2013).
[30] Miller C.L., Lai B. Human and mouse hematopoietic colony-forming cell assays. Basic Cell Culture Protocols 3, Methods in Molecular Biology, vol 290. (eds. Helgason CD, Miller CL) Humana Press, Totowa, NJ. pp71-89. (2005).
[31]Davidson, A.J., Zon, L.I. The 'definitive' (and 'primitive') guide to zebrafish hematopoiesis. *Oncogene* **23**, 7233–7246, (2004).
[32]de Jong, J.L., Zon, L.I. Use of the zebrafish system to study primitive and definitive hematopoiesis. *Annu Rev Genet* **39**, 481–501, (2005).

[33] He, B.L., Shi, X., Man, C.H., Ma, A.C., *et al.* Functions of flt3 in zebrafish hematopoiesis and its relevance to human acute myeloid leukemia *Blood* **123**, 2518–2529, (2014).
[34] Gajiwala, K.S., *et al.* KIT kinase mutants show unique mechanisms of drug resistance to imatinib and sunitinib in gastrointestinal stromal tumor patients *Proc. Natl. Acad. Sci. USA* **106**, 1542–1547, (2009).
[35] Smith CC, *et al.* Activity of ponatinib against clinically-relevant AC220-resistant kinase domain mutants of FLT3-ITD. *Blood*. **121**, 3165–3171, 2013.
[36] For a recent example of rationally designed polypharmacology, see: Ciceri, P. *et al.* Dual kinase-bromodomain inhibitors for rationally designed polypharmacology *Nat. Chem. Biol.* **10**, 305–314, (2014).
[37] Griswold I.J., *et al.* Effects of MLN518, a dual FLT3 and KIT inhibitor, on normal and malignant hematopoiesis. *Blood*. **104**, 2912–2918, (2004).
[38] Chen Z., Buki K., Vääräniemi J., Gu G. & Väänänen H.K. The critical role of IL-34 in osteoclastogenesis. *PLoS One.* **6**, (2011).
[39] Huynh, D., *et al.* CSF-1 Receptor-Dependent Colon Development, Homeostasis and Inflammatory Stress Response *PLoS ONE* **8**, e56951, (2013).
[40] Stanley E.R., *et al*. Biology and action of colony--stimulating factor-1. *Mol. Reprod. Dev.* **46**, 4–10, (1997).
[41] Thiede, M.A., *et al.* Thrombocytopenia in the toothless (osteopetrotic) rat and its rescue by treatment with colony-stimulating factor-1 *Exp. Hematol.* **24**, 722–727, (1996).
[42] Dai, X.-M., *et al.* Targeted disruption of the mouse colony-stimulating factor 1 receptor gene results in osteopetrosis, mononuclear phagocyte deficiency, increased primitive progenitor cell frequencies, and reproductive defects *Blood* **99** 111–120, (2002).
[43] Ramos, M.I., Pak, P.P., Lebre, M.C. Fms-like tyrosine kinase 3 ligand-dependent dendritic cells in autoimmune inflammation *Autoimmunity Reviews* **13**, 117–124, (2014).
[44] Bollag, G., *et al.* Clinical efficacy of a RAF inhibitor needs broad target blockade in BRAF-mutant melanoma *Nature* **467**, 596–599, (2010).
[45] Anastassiadis, T., *et al.* Comprehensive assay of kinase catalytic activity reveals features of kinase inhibitor selectivity *Nat. Biotechnol.* **29**, 1039–1045, (2011).

Figure Legends

Figure 1. **Purified kinase assays comparing SAR of staralogs**. (**A**) PKC412 (N-benzoylstaurosporine) potently inhibits all Class III/PDGFR family hematopoietic stem cell kinases. Staurosporine analog (staralogs) Star 12, with large alkyl C7 (R_1) substituent is a weak inhibitor of FLT3 but suggested more selectivity for Class III RTKs. (**B**) Table shows purified kinase in vitro assays testing SAR showing optimal potency at R_1 = methyl; rigid potency window found with Star 27 with n-propyl-NH_2 at R_2 but not R_3. Star ## ordered by increasing potency and numbering consistent with prior usage.[27] Error ranges represent standard error of the mean (SEM) and are the result of at least three independent measurements, each in triplicate. (**C**) IC_{50} values of PKC412 and lead

compounds Star 23 and 27 against the hematopoietically relevant five Class III RTKs showing the optimal selectivity achieved for Star 27. Log_{10}-scale heat map highlights IC_{50} ratios relative to FLT3, indicating progression from PKC412 having lower selectivity towards Star 27 having high selectivity. (**D**) Dendrogram showing single point inhibition for 319 kinases for PKC412. Each value represents the average of two experiments ± SEM (performed by RBC). (**E**) Dendrogram showing single point inhibition for 319 kinases for Star 27. (**F**) Graph of Tyr kinases. y-axis = potency by single point for Star 27 as a function of the corresponding potency with PKC412.

Figure 2. (**A**) **Table of cellular EC50 values for leading experimental clinical therapies** (Sorafenib, AC220, Ponatinib, and PKC412) and Star 27 against a panel of AML-relevant human-derived (MV4;11 and molm14) cell lines and toxicity controls (HMC1.1 and K562) (adapted* from Refs. 28, 29, and 35). Star 27 shows a similar order of magnitude potency against Molm14 and MV4;11 compared to PKC412. Relevant therapeutic windows between PKC412 and Star 27: an over 5-fold increase in selectivity for HMC1.1/MV4;11 cells and an 11-fold increase for HMC1.1/Molm14 is observed for Star 27 over PKC412. Replicates shown are the result of at least three attempts, each in triplicate, and error ranges represent the standard error of the mean. (**B**) Normalized caspase-3 negative cells plotted against escalating drug dosage. Star 27 shows a similar degree of apoptosis to PKC412 in Molm14 cells. (**C**) In KIT-addicted HMC1.1 cells PKC412 exhibits potent toxicity while Star 27 shows very little even up to 2,500 nM. Results performed in triplicate with two biological replicates. ** $P < 0.01$; *** $P < 0.001$. (**D**) PKC412 and Star 27 have a similar degree of inhibition against p-FLT3 in Molm14

cells as well as a similar degree for p-STAT5 and p-S6 (for p-ERK, p-AKT, and p-MEK, data not shown). In the HMC1.1 cells, by contrast, PKC412 and Star 27 show a larger difference in p-KIT inhibition.

Figure 3. Colony forming assays comparing effect of Star 27 and PKC412 on normal donor-derived stimulated peripheral blood (SPB), normal bone marrow (BM) growth, and malignant blast reduction. (**A**,**B**,**C**) Colony forming assays comparing effects of Star 27 and PKC412 on primary patient AML circulating blast growth in methylcellulose. Colonies consist primarily of leukemic blasts of various hematopoietic identities. BFU colonies are not shown. Colony numbers scored individually for each replicate 3 cm plate. (**A**) Images showing leukemic blast morphology in DMSO-treated plates and representative images in 1,000 nM-treated plates for both drugs as indicated. (**B**) Primary patient FLT3 ITD+ AML circulating blasts. Raw colony numbers range from ca. 20 in PKC412 or Star 27-treated cells at 1,000 nM to ca. 1,200 for CFUs in DMSO-treated plates. Concentrations shown were applied in triplicate to each concentration for two different cell densities, the larger (2.5 x 10^5 cells/mL) showing adequate cell growth and colony formation for statistically significant counts, the averages of those trails then calculated for standard error of the mean. * $P < 0.05$. (**c**) Primary patient FLT3 D835Y AML circulating blasts. Raw colony numbers range from ca. 25 for PKC412 (or 50 for Star 27) at 1,000 nM to ca. 120 for DMSO-treated plates. Conditions repeated in duplicate or higher replicates. Colonies scored individually for the highest cell density tested (2.5 x 10^5 cells/mL). Similar to primary ITD patient samples, colonies consist mostly of poly-hematopoietic leukemic blasts. * $P < 0.05$. (**D**,**E**,**F**) Normal BM and SPB

colony data. (**D**) Images of colonies grown and derived from normal BM (images of SPB not shown) in methylcellulose. Raw colony numbers for BM range from zero in most PKC412-treated replicates at 1,000 nM to ca. 400 for BFUs and ca. 300 for CFUs in all Star 27-treated conditions. Non-magnified differences are particularly noticeable between the 1,000 nM and 250 nM dosages. (**E**,**F**) Concentrations shown were applied in triplicate to three normal SPB and one normal BM donors, the averages of those trials then calculated for standard error of the mean (full data not shown). Colony counts for DMSO ranged from the low 100's to 400's. Graphs show Star 27 having no effect on hematopoiesis up to 1,000 nM while PKC412 eliminates most normal hematopoietic colony forming potential at 1 mM on colony forming units (CFU) and blood forming units (BFU), respectively. CFU-GEMM colonies were counted as one CFU plus one BFU. * $P < 0.05$; *** $P < 0.001$.

Figure 4. Effects of Star 27 on *D. rario* (zebrafish) WT morphology and myelopoiesis, and FLT3-ITD AML context. Effect of Star 27 on zebrafish normal myelopoiesis and the FLT3/ITD-induced myeloid cells expansion. (**A**-**D**) The effect of Star 27 on zebrafish embryonic development at 3 dpf, showing no noticeable morphological defects up to 10 μ M. (**E**-**I**) The effect of PKC412 on zebrafish embryonic development at 3 dpf, showing substantial pericardial defects beginning at 500 nM (data not shown), and tail curvature and length defects beginning at 1 μ M and 2.5 μ M, respectively vs. vehicle. (**J**,**K**,**M**) The effect of 10 μ M Star 27 treatment on mpo+ myeloid cells development in the posterior blood island (PBI) at 30 hpf, showing no statistically significant change. (**J**,**L**,**M**) The effect of 10 μ M PKC412 treatment on mpo+

myeloid cells development in the posterior blood island (PBI) at 30 hpf, showing a statistically significant granulogenesis/myelosuppression. (**N**-**P**) Three categories of *mpo* transcription (**N**, normal; **O**, intermediate; **P**, Severe) were defined based on the WISH results (three experiments). (**Q**) The rescue effect of 10 μ M Star 27 treatment on FLT3/ITD-induced mpo+ myeloid cells expansion at 30 hpf, showing rescue of normal phenotype approaching that seen for AC220.[33] Scale bar equals 500 μ m. Blue arrows indicate the pericardial edema, red arrows indicate tail shortening and curving, and red arrows indicate the FLT3-ITD AML mpo+ myeloid cells expansion. PKC412 treatment on FLT3/ITD-induced mpo+ myeloid cells expansion at 30 hpf, showing an efficaciousness similar to Star 27, consistent with Figs. 1-3. For all experiments: Zebrafish embryos were collected and kept in standard E3 medium at 28 ℃. Different concentrations of either drug were added to the E3 medium from 6 hours-post fertilization (hpf) to 3 days-post fertilization (dpf). Embryos treated with DMSO or 10 μ M drug from 6 to 30 hpf were collected for *mpo* whole mount in situ hybridization (WISH) analysis. 80 ng plasmid DNA containing FLT3/ITD sequence was microinjected into one-cell stage embryos, and the uninjected embryos were used as control. FLT3/ITD-injected embryos were treated with DMSO or 10 μ M drug from 6 to 30 hpf. Embryos were collected at 30 hpf for *mpo* WISH analysis. ** $p < 0.01$.

Figure 5. Electronic model of selectivity. Star 27-des methyl (PKC412-relevant) and Star 27 are depicted in 3D with electron potential mapping (EPM) to highlight the difference of a single methyl group. (**A**-**C**) Star 27-des methyl maintains a partial

positive charge at the C7 position which matches the partial negative charge on the Thr 670 gatekeeper of KIT, potentially explaining PKC412's relative affinity for KIT. (**D**-**F**) Star 27 maintains a neutral charged surface at C7 due to the presence of the methyl group, potentially explaining its lack of binding to KIT.

Figure 6. Heatmap of cellular EC_{50} values for leading clinical therapies (S = Sorafenib, A = AC220, P = Ponatinib, PKC412) and Star 27 against a panel of AML-relevant human- and mouse-derived drug-resistant cell lines (**A**) (adapted from Refs. 28, 29, and 35). Log_{10}-scale fold resistance between Ba/F3 FLT3 ITD and drug-induced mutations (ITD + TKD double mutant) shown via heat map. Point mutations corresponding to each drug-relevant resistance shown. Star 27 maintains potency between FLT3 ITD and resistance mutants comparable to PKC412, including the resistance mutant of PKC412, itself. Mutations derived independently from both saturating mutagenesis and patient-derived samples.[9] Replicates shown are the result of at least two or three attempts, each in triplicate, and error ranges represent the standard error of the mean. (**B**,**C**) Crenolanib's effect on p-KIT inhibition and of colony growth in normal BM. (**B**) Crenolanib inhibits p-KIT in HMC1.1 cells at 12 nM IC_{50}. This level of inhibition translates to downstream kinases, with inhibition of p-AKT (S473) and p-S6 (S235/S236). (**C**) Crenolanib potently inhibits normal BM colony formation at <63 nM and 63 nM IC_{50}'s of CFU and BFU colonies, respectively.

Figure 1

A

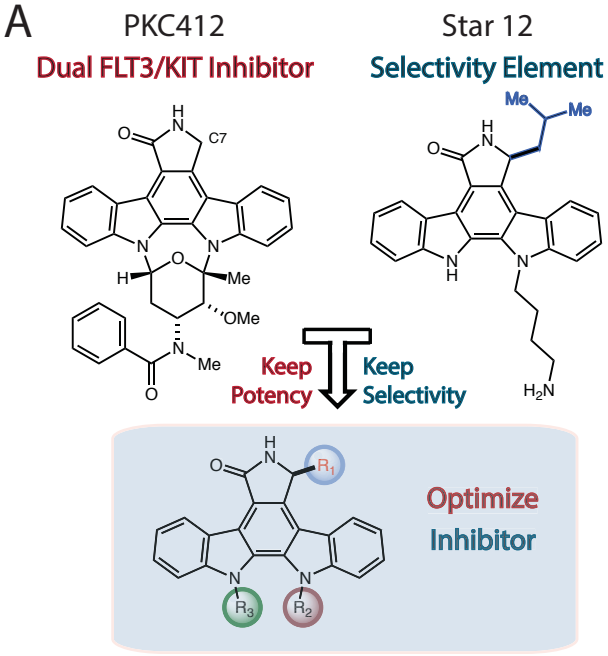

B

Star #	R_1	R_2	R_3	IC_{50} FLT3 (nM)
Star 7	t-Bu	H	H	>10,000
Star 3	n-Pr	H	H	>10,000
Star 1	i-Bu	H	H	>10,000
Star 4	n-Bu	H	H	>10,000
Star 9	propargyl	H	H	>10,000
Star 6	i-Pr	H	H	2,000
Star 8	Et	H	H	2,000
Star 22	Me	H	H	193 ± 28
Star 12	i-Bu	n-Butyl-NH_2	H	524 ± 94
Star 23	Me	n-Butyl-NH_2	H	10 ± 4
Star 27	**Me**	**n-Propyl-NH_2**	**H**	**1.5 ± 1**
Star 27-iso	Me	H	n-Propyl-NH2	15 ± 7
PKC412	H	sugar	sugar	2 ± 1

C

Class III RTK	IC_{50} (nM) PKC412	Star 23	Star 27	Gatekeeper
FLT3	<0.5	9 ± 1	<0.6 ± 0.1	Phenyl Alanine
CSF1R	4 ± 0.4	>10,000	>9,880 ± 120	Threonine
KIT	36 ± 1	6,550 ± 160	1,020 ± 10	Threonine
PDGFRα	9 ± 1	2,005 ± 125	931 ± 109	Threonine
PDGFRβ	14 ± 2	2,800 ± 40	80 ± 11	Threonine
KIT / FLT3	>72	728	>1,700	

0.9 — 4.2 Log_{10}-fold selectivity vs. FLT3

D

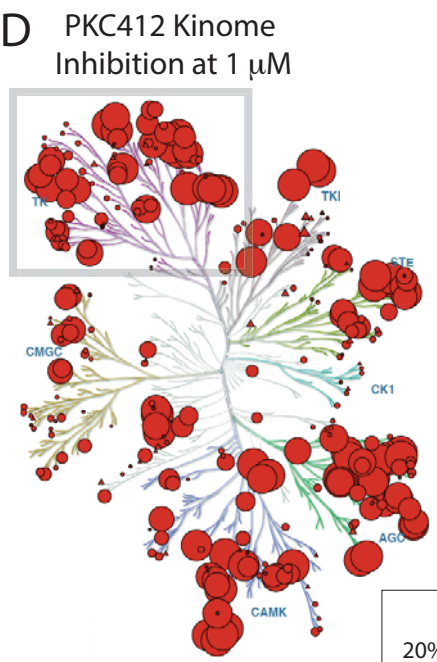

E

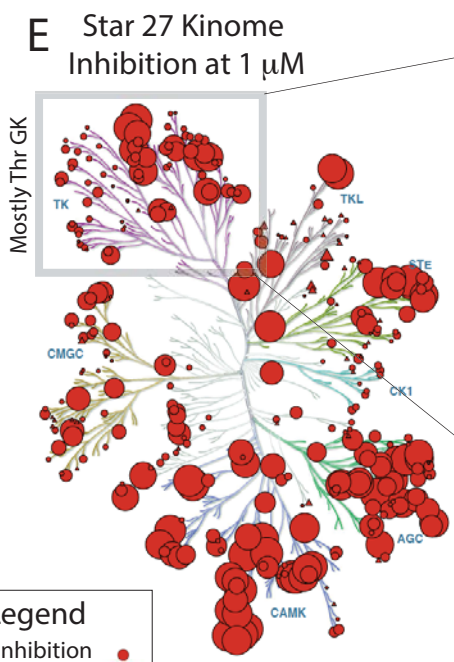

Legend
20% inhibition
60% inhibition
100% inhibition

F

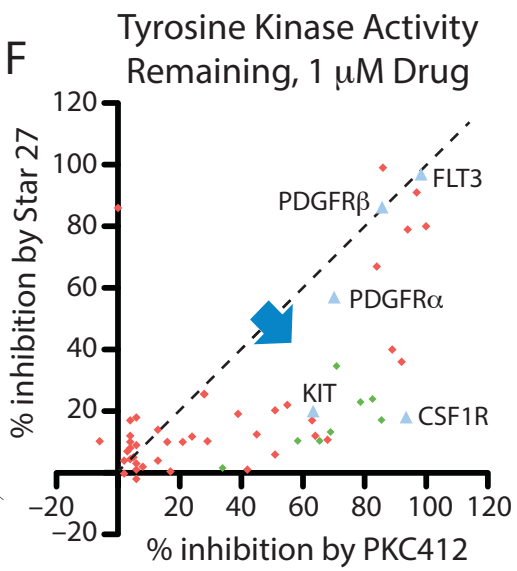

Class III RTKs
Src Family
Other Tyr Kinases

Figure 2

A

Cell Line	Driver Mutation	IC_{50} (nM) Sorafenib*	AC220*	Ponatinib*	PKC412	Star 27
Molm14	FLT3-ITD (heterozygous)	68	<5	--	37 ± 7	57 ± 8
MV4;11	FLT3-ITD (homozygous)	4	<5	2	16 ± 5	41 ± 6
HMC1.1	Kit V560 G	58	5	<10	354 ± 60	>5,000
K562	Bcr-Abl	>5,000	>1,000	5	>5,000	>5,000

*see refs. 28, 29, and 35 for values

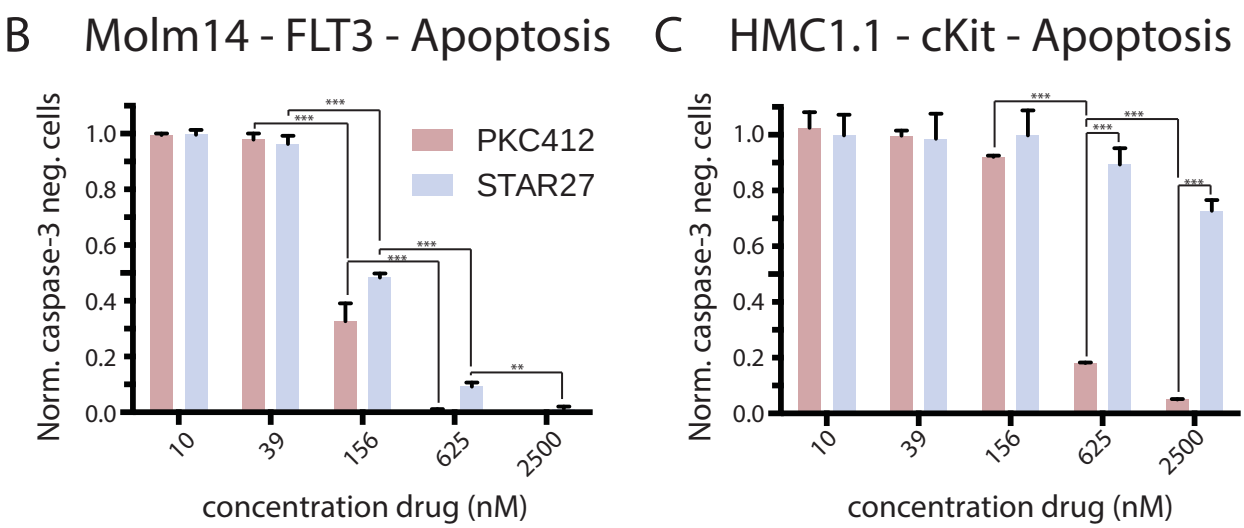

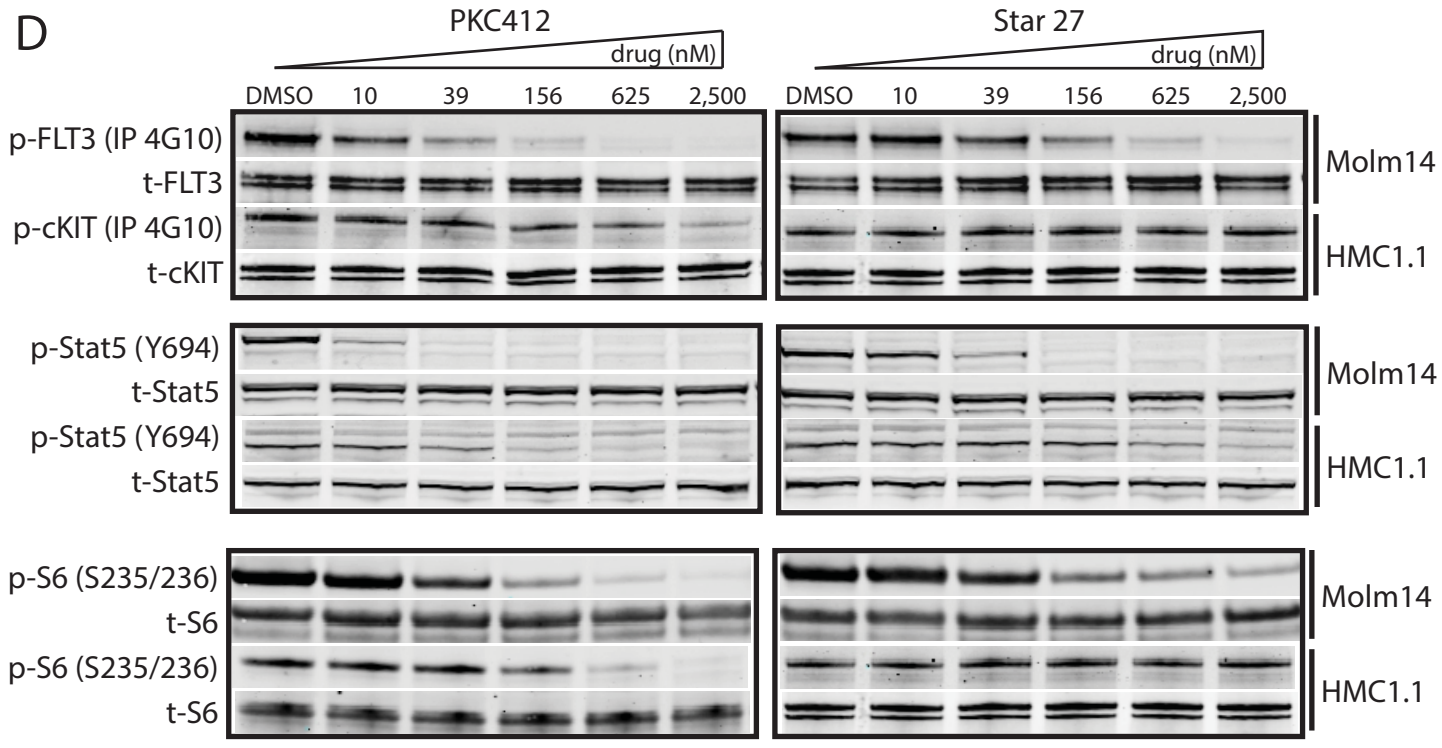

Figure 3

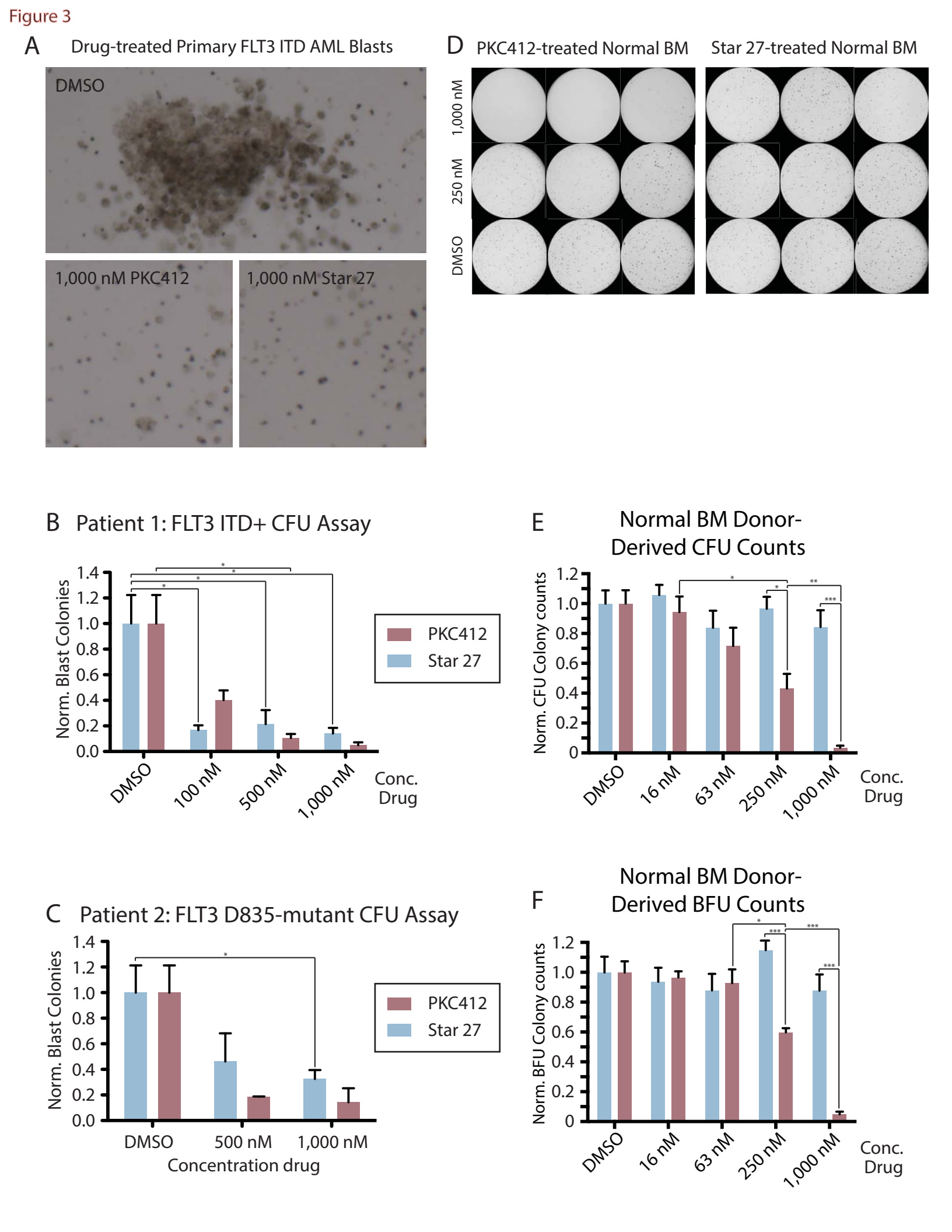
A
Drug-treated Primary FLT3 ITD AML Blasts
DMSO
1,000 nM PKC412
1,000 nM Star 27
D
PKC412-treated Normal BM
Star 27-treated Normal BM
1,000 nM
250 nM
DMSO
B
Patient 1: FLT3 ITD+ CFU Assay
Norm. Blast Colonies
1.4
1.2
1.0
0.8
0.6
0.4
0.2
0.0
DMSO
100 nM
500 nM
1,000 nM
Conc. Drug
PKC412
Star 27
E
Normal BM Donor-Derived CFU Counts
Norm. CFU Colony counts
1.2
1.0
0.8
0.6
0.4
0.2
0
DMSO
16 nM
63 nM
250 nM
1,000 nM
Conc. Drug
C
Patient 2: FLT3 D835-mutant CFU Assay
Norm. Blast Colonies
1.4
1.2
1.0
0.8
0.6
0.4
0.2
0.0
DMSO
500 nM
1,000 nM
Concentration drug
PKC412
Star 27
F
Normal BM Donor-Derived BFU Counts
Norm. BFU Colony counts
1.2
1.0
0.8
0.6
0.4
0.2
0
DMSO
16 nM
63 nM
250 nM
1,000 nM
Conc. Drug

Figure 4

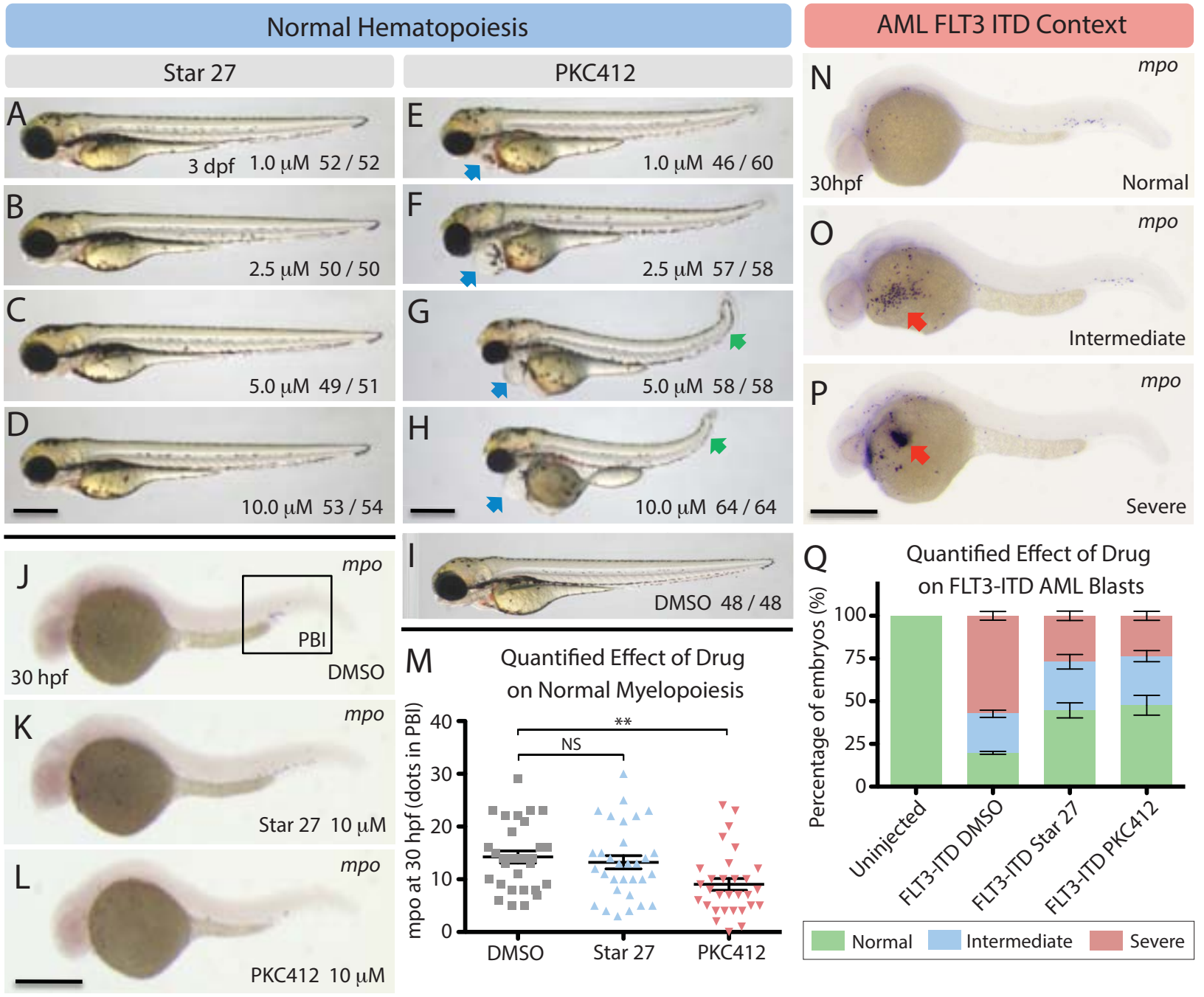
Normal Hematopoiesis
AML FLT3 ITD Context
Star 27
PKC412
A
3 dpf 1.0 μM 52 / 52
B
2.5 μM 50 / 50
C
5.0 μM 49 / 51
D
10.0 μM 53 / 54
E
1.0 μM 46 / 60
F
2.5 μM 57 / 58
G
5.0 μM 58 / 58
H
10.0 μM 64 / 64
I
DMSO 48 / 48
J
mpo
PBI
30 hpf
DMSO
K
mpo
Star 27 10 μM
L
mpo
PKC412 10 μM
M
Quantified Effect of Drug
on Normal Myelopoiesis
mpo at 30 hpf (dots in PBI)
40
30
20
10
0
**
NS
DMSO
Star 27
PKC412
N
mpo
30hpf
Normal
O
mpo
Intermediate
P
mpo
Severe
Q
Quantified Effect of Drug
on FLT3-ITD AML Blasts
Percentage of embryos (%)
100
75
50
25
0
Uninjected
FLT3-ITD DMSO
FLT3-ITD Star 27
FLT3-ITD PKC412
Normal
Intermediate
Severe

Figure 5.

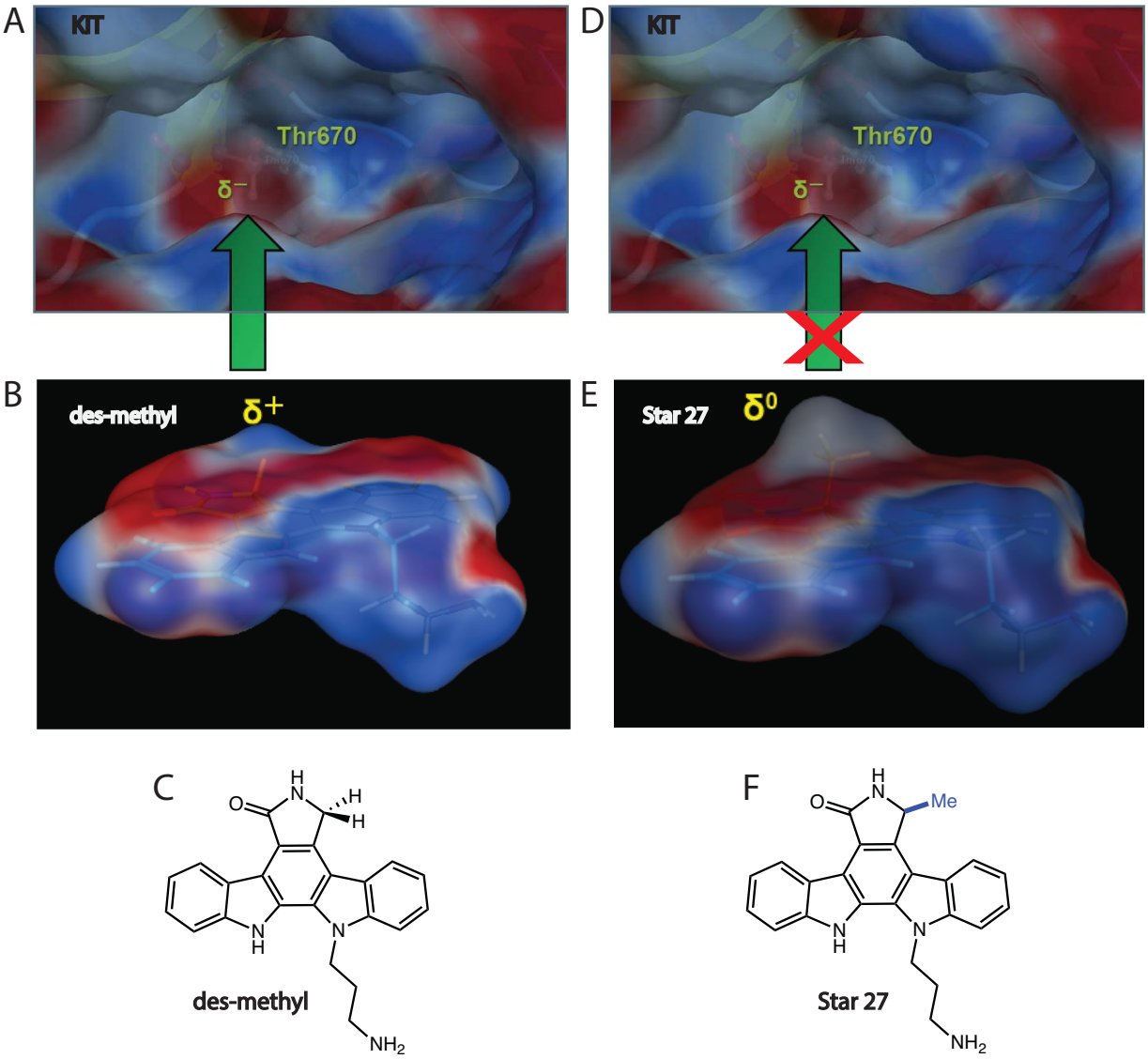
A
KIT
Thr670
δ−
D
KIT
Thr670
δ−
B
des-methyl
δ+
E
Star 27
δ0
C
des-methyl
F
Star 27
Me

Figure 6

A

Cell Line	Drug Resistance	IC_{50} (nM) Sorafenib*	AC220*	Ponatinib*	PKC412	Star 27
Parental + IL3	--	8,785 ± 1,966	>1,000	>1,000	243 ± 73	2,300 ± 1,200
FLT3 ITD	--	3.2 ± 0.9	0.38 ± 0.04	1.4 ± 1.1	6 ± 4	57 ± 45
FLT3 D835V	--	ND	ND	ND	<5	19 ± 3
FLT3 D835Y	--	ND	ND	ND	<5	18 ± 12
FLT3 ITD + D835V	A, P	2,429 ± 229	179 ± 11	262 ± 7.7	8 ± 5	70 ± 58
FLT3 ITD + D835Y	A, P	675	28	284	6 ± 3	39 ± 24
FLT3 ITD + D835F	A, P	2,374	166	414	9 ± 3	53 ± 36
FLT3 ITD + D835H	A, P, S	164	6	211	7 ± 2	48 ± 29
FLT3 ITD + Y842H	A	260	18	80	5 ± 1	38 ± 24
FLT3 ITD + Y842C	A, P	469	33	229	5 ± 2	48 ± 29
FLT3 ITD + D839G	P	112	2	54	10 ± 3	80 ± 41
FLT3 ITD + F691L	A, P	2,526 ± 144	151 ± 8.2	49.3 ± 1.0	8 ± 4	144 ± 97
FLT3 ITD + D698N	C	6.1 ± 2.3	0.58 ± 0.1	2.02 ± 1.1	34 ± 21	174 ± 44
FLT3 ITD + Y693C	C	57.4 ± 14.3	2.2 ± 0.2	19.9 ± 2.0	119 ± 44	279 ± 36
FLT3 ITD + A848P	A, S	ND	12	ND	9 ± 6	53 ± 31

Activation loop
Nucleotide binding site

A = AC220, P = Ponatinib, S = Sorabenib, PKC = PKC412, C = Crenolanib

−0.5 +3.4 Log_{10}-fold resistance over FLT3 ITD

*IC50 values adapted from references 28, 29 and 35 for A, P, and S.

B

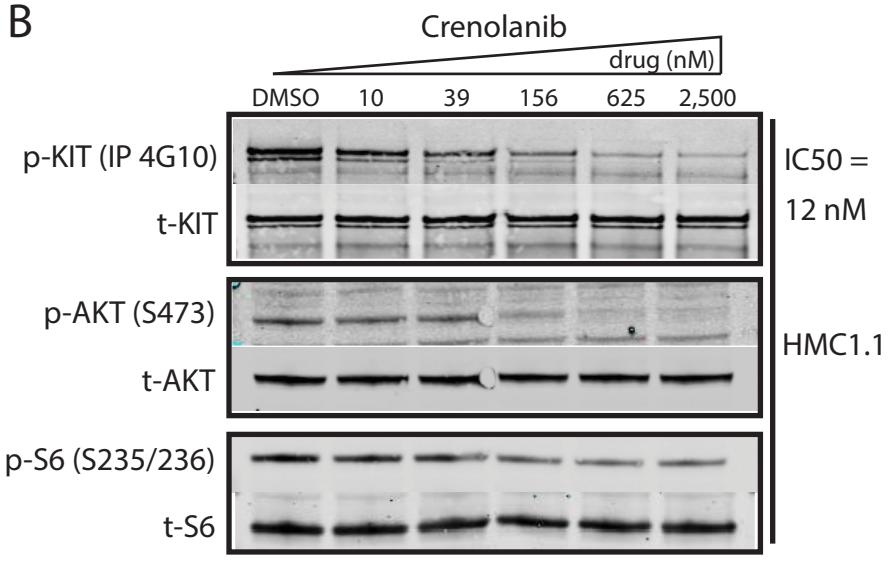

C